

# 1 Transformations in Exposure to Debris Flows in Post-Earthquake Sichuan, 2 China

3  
4 Isabelle Utley<sup>1</sup>, Tristram Hales<sup>1</sup>, Ekbal Hussain<sup>2</sup>, Xuanmei Fan<sup>3</sup>

5  
6 [1] School of Earth and Environmental Sciences, Cardiff University, Cardiff, CF10 3AT, UK.

7 [2] British Geological Survey, Keyworth, Nottingham, NG12 5GG, UK

8 [3] State Key laboratory of Geohazard Prevention, Chengdu University of Technology, Chengdu, China

9  
10 *Correspondence to: Isabelle E.K Utley (utleyieu@gmail.com)*

11  
12 **Abstract.** Post-earthquake debris flows can exceed volumes of  $1 \times 10^6 \text{m}^3$  and pose significant challenges to  
13 downslope recovery zones. These stochastic hazards form when intense rain remobilises coseismic landslide  
14 material. As communities recover from earthquakes they mitigate the effects of these debris flows through  
15 modifications to catchments such as building check dams and levees. We investigate how different catchment  
16 interventions change exposure and hazard of post-2008 debris flows in three gullies in Sichuan province, China.  
17 These were selected based on the number of post-earthquake check dams – Cutou (2), Chediguan (2) and Xiaoja  
18 (none). Using high resolution satellite images, we developed a multitemporal building inventory from 2005 to  
19 2019, comparing it to spatial distribution of previous debris flows and future modelled events. Post-earthquake  
20 urban development in Cutou and Chediguan increased exposure to a major debris flow in 2019 with inundation  
21 impacting 40% and 7% of surveyed structures respectively. We simulated future debris flow runouts using  
22 LAHARZ to investigate the role of check dams in mitigating three flow volumes –  $10^4 \text{m}^3$  (low),  $10^5 \text{m}^3$  (high)  
23 and  $10^6 \text{m}^3$  (extreme). Our simulations show check dams effectively mitigate exposure to low and high flow  
24 events but prove ineffective for extreme events with 59% of buildings in Cutou, 22% in Chediguan and 33% in  
25 Xiaoja significantly affected. We verified our analyses through employing a statistical exposure model, adapted  
26 from a social vulnerability equation. Cutou's exposure increased by 64% in 2019, Chediguan's by 52% whilst  
27 only 2% for Xiaoja in 2011, highlighting that extensive grey infrastructure correlates with higher exposure to  
28 extreme debris flows, but less so to smaller events. Our work suggests the presence of check dams increases the  
29 perception of exposure reduction downstream, however, ultimately produces a levee effect that raises exposure to  
30 large events.

## 31 **Keywords**

32 Debris Flows, Built Environment, Exposure, Check dams, LAHARZ.

## 33 **1. Introduction**

34  
35  
36 Major earthquakes such as the 1994  $M_w$  6.8 event in Northridge, California (Harp and Jibson, 1996) and the 1999  
37  $M_w$  7.3 earthquake in Chi-Chi, Taiwan (Liu et al., 2008) have triggered chains of hazards that increase the exposure  
38 of local communities to secondary hazards for many years after the initial disaster. Following the 2008  $M_w$  7.9  
39 Wenchuan earthquake in Sichuan, China, debris flows occurred more frequently and at a higher magnitude ( $>1 \times$   
40  $10^6 \text{m}^3$ ) after the earthquake compared to flows before the earthquake (Cruden and Varnes., 1996; Cui et al., 2008;  
41 Huang and Li., 2009; Guo et al., 2016; Thouret et al., 2020). Increased debris flow frequency impacts vulnerable  
42 communities and local infrastructure, potentially reshaping the demographic and structural landscape of  
43 previously rural regions (Chen et al., 2011). The frequency of post-seismic flows is heavily influenced by sediment  
44 availability, often controlled by coseismic landslide distribution, hydrology, and slope (Horton et al., 2019). The  
45 ready transformation and remobilisation of seismically loosened deposits into water-laden sediments leads to a  
46 heightened probability of debris flow hazards for extended periods, further exacerbating the potential impacts felt  
47 by these areas (Costa et al., 1984; Huang & Li, 2014; Fan et al., 2019b).

48  
49  
50 Post-seismic debris flows affect the expanding built environment and communities located in the flat land that  
51 forms along floodplains and on debris and alluvial fans. In addition to direct loss of life, debris flows repeatedly  
52 block and/or destroy rivers, roads, tunnels, and bridges, and damage property and agriculture, and result in loss of  
53 life (Chen, N et al., 2011). Buildings are particularly susceptible to the impacts of debris flows (Hu et al., 2012;  
54 Zeng et al., 2015), with property damage accounting for nearly all impacts such as casualties and fatalities (Wei  
55 et al., 2018; Wei et al., 2022). Variations in construction materials are a particularly important factor in  
56 determining structural resilience and vulnerability to debris flows (Zhang, S et al., 2018). Despite focus on  
57 building resilience and reducing vulnerability, post-earthquake regions are often areas of significant rebuilding  
58 and expansion of infrastructure so the exposure to debris flows changes rapidly in these areas. The development

59 of critical infrastructure such as highways and tunnels further encourages the growth of the built environment and  
60 subsequent influx of people settling in areas exposed to geological hazards (Cruden and Varnes, 1996; Jiang et  
61 al., 2016).

62  
63 Check dams are a common form of risk mitigation for debris flows globally (Zeng et al., 2009; Peng et al., 2014;  
64 Cucchiaro, S. et al., 2019b), and one that is prevalent in post-earthquake Wenchuan (Chen, X. et al., 2015; Guo  
65 et al., 2016). Check dams store debris flow sediment, locally reduce channel slope, and are often permeable to  
66 affect debris flow hydrology. However, they have disadvantages such as requiring regular maintenance (to reduce  
67 sediment inputs) (Kean et al., 2018). The mitigation potential of these structures is contingent on their position  
68 along a channel, their height, amount of sediment fill, and their strength (which depends on the materials used for  
69 construction) (Dai et al., 2017). These factors evolve through time, meaning that the hazard-mitigating factor of  
70 check dams can vary with time and often with unpredictable results. The presence of check dams changes the  
71 downstream risk, primarily by altering the magnitude and frequency distribution of debris flows within the  
72 channel. For well-made check dams of sufficient volume to mitigate the largest debris flows, this can reduce the  
73 downstream risk of debris flows to negligible by effectively mitigating the entire hazard. However, in the case of  
74 the Wenchuan region, check dams are rarely large enough or regularly cleared of sediment to mitigate the largest  
75 debris flows, which can exceed  $10^6 \text{ m}^3$  in volume.

76  
77 The presence of check dams, particularly in drainage basins with a limited history of catastrophic debris flow  
78 events, may affect the perception of risk downstream. They serve to stabilize, obstruct, drain, and/or halt the  
79 movement of flows (Hübl and Fiebigger., 2005; Chen et al., 2015). The perception that check dams have mitigated  
80 all hazards may promote the expansion of infrastructure into floodplains and debris fans, potentially increasing  
81 exposure to debris flows that overtop dams or occur due to dam failure. The increase of exposure is common on  
82 floodplains where the presence of flood control levees can promote building onto floodplains – a process known  
83 as the levee effect (Collenteur et al., 2015). In the flooding example, the presence of levees reduces the frequency  
84 of small and medium sized floods, but when large floods occur that cause those levees to fail, heightened  
85 floodplain exposure can lead to higher damage. The effect of check dams on risk perception is less well  
86 understood. Anecdotal examples from the Wenchuan region (e.g., Hongchun, Taoguan gullies) show that large  
87 debris flow events in 2010, 2013 and 2019 caused significant damage despite the presence of check dams (Dai et  
88 al., 2017). However, it is not clear if the presence of check dams affected exposure relative to the large-scale  
89 expansion of infrastructure in the post-earthquake recovery phase.

90  
91 This study seeks to understand whether the addition of engineered mitigation measures, primarily check dams,  
92 have influenced the susceptibility of post-earthquake Wenchuan communities to large debris flows. We compare  
93 3 catchments with similar topography and geology, but different levels of mitigation. We measure the building  
94 exposure in two neighbouring catchments with check dams (Cutou and Chediguan) and compare with a third,  
95 unmitigated gully (Xiaojia). We examine how infrastructure develops in the basins with time and as a function of  
96 check dam measures. By analysing infrastructure development in these catchments, particularly in Cutou and  
97 Chediguan in the years following mitigation – will seek to assess how check dam construction has impacted  
98 infrastructure growth and the potential exposure to debris flow events of different sizes. Additionally, our analysis  
99 will explore whether the presence of these structures has impacted risk perception and/or land-use decisions in  
100 ‘at-risk’ catchments.

## 101 102 103 **2. Study Area: Sichuan Province, China**

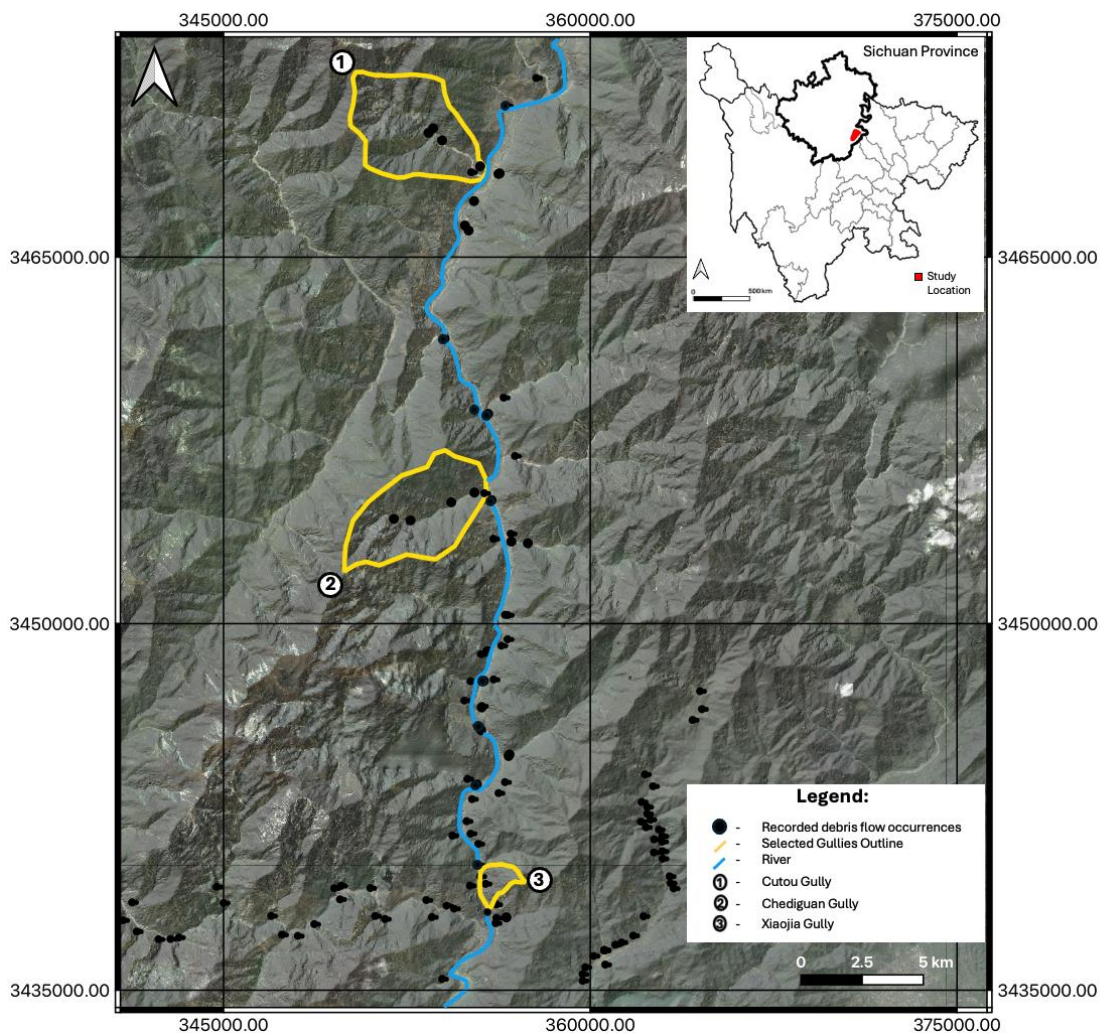
104 China’s mountainous regions, including the Longmenshan, account for 69% of the country’s land mass with over  
105 a third of the population living in these regions (Chen et al., 2011; He et al., 2022). 72% of this landscape suffers  
106 from debris flow activity. Between 2005 and 2018, estimates suggest over 800 debris flow occurrences each year  
107 (He et al., 2022; Wei et al., 2021). Of these, landslides dominate provinces in the North and debris flows are  
108 generally constrained to provinces in the South (Liu et al., 2018). The 2008  $M_w$  7.9 Wenchuan earthquake  
109 primarily impacted Sichuan province (Fig 1). The epicentre was located near Yinxiu, Wenchuan County, within  
110 the seismically active Longmenshan Fault Zone (Li et al., 2019). The shaking triggered around 56,000 landslides  
111 and displaced nearly  $3 \text{ km}^3$  of loose material (Fan et al., 2018; Luo et al, 2020). In subsequent years, the unstable  
112 material has been reactivated as debris flows, many of which exceed  $10^6 \text{ m}^3$  in mobilised volume (Frances et al.,  
113 2022). The risk from these debris flows has been compounded by increasing exposure due to China’s rapid rural  
114 development programme, which includes the construction of roads, bridges, and industrial facilities (Tang et al.,  
115 2022).

116  
117 Four significant episodes of debris flows occurred in the post-earthquake Wenchuan region in 2008, 2010, 2013  
118 and 2019 (Tang et al., 2022; Fan et al., 2019b). Each event was associated with monsoon rainfall that occurred in

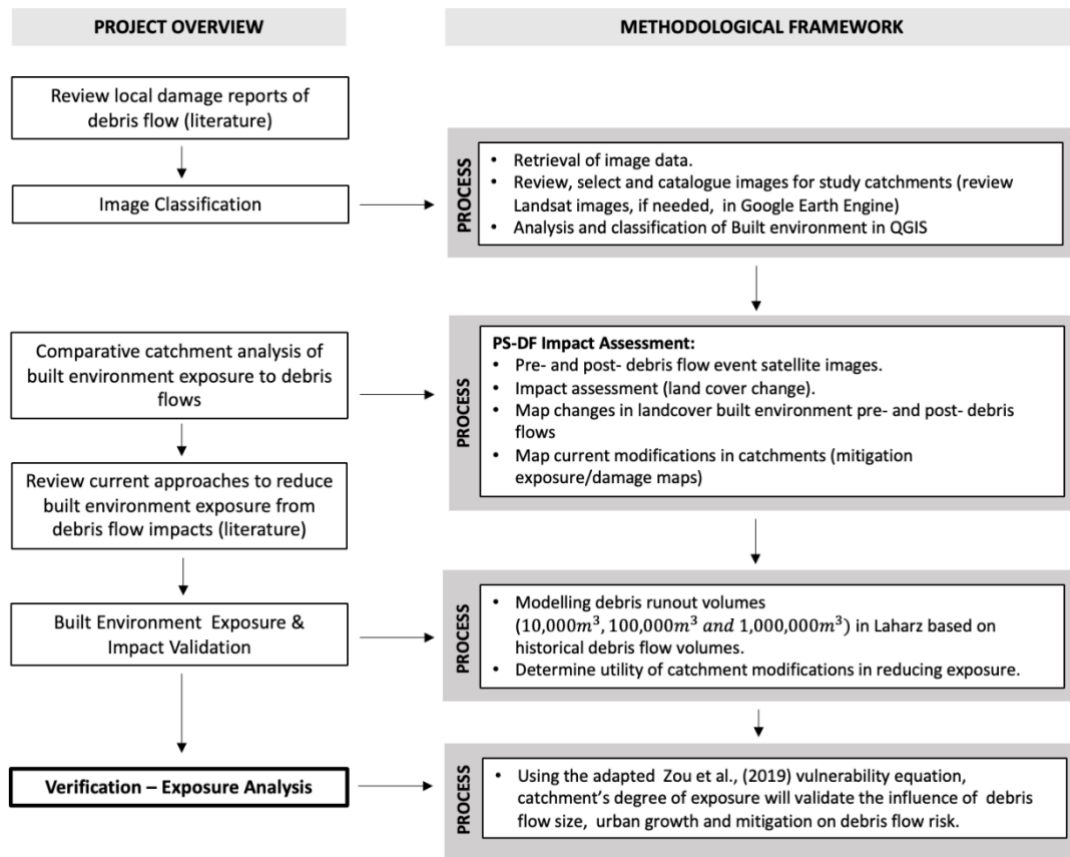
119 different parts of the range. The largest flow surges, containing millions of cubic meters of sediment were located  
120 in the gullies along the Minjiang in Sichuan. Large scale flooding further amplified the impacts, for example in  
121 Yingxiu Town, Wenchuan County (Liu et al., 2016b). Debris flow events occurring post-earthquake often exhibit  
122 larger material volumes compared to flow events recorded prior to 2008. Horton et al., (2019) attributed the  
123 increase in flow volume to high in channel sediment volumes that can drive bulking. The resulting increase in  
124 debris flow hazards necessitated engineered mitigation measures to reduce risk levels in the basin communities  
125 (Tang et al., 2009; Huang et al., 2009; Huang, 2012).

127 In this study we focus on three gullies along the Minjiang - Cutou, Chediguan and Xiaojia and debris flow events  
128 on August 20<sup>th</sup>, 2019, and 4<sup>th</sup> July 2011 (Fig 1). Cumulative rainfall on 20<sup>th</sup> August 2019 peaked at 83 mm in  
129 Cutou and 65 mm in Chediguan resulting in large debris flows measuring over  $50 \times 10^4 \text{ m}^3$  in each gully. Cutou  
130 gully is known for its high frequency of post-seismic debris flows, which has been attributed to the total of  $11 \times 10^6$   
131  $\text{m}^3$  coseismic deposits generated by the earthquake (Yan et al 2014). Although a check dam was built in 2011 to  
132 manage debris flow impacts in Chediguan gully a large damaging debris flow of  $64 \times 10^4 \text{ m}^3$  occurred on 20 August  
133 2019 and destroyed the drainage groove and G213 Taiping Middle Bridge (Li et al., 2021). The debris briefly  
134 blocked river flow in the Minjiang causing water levels to rise during flood peak. This led to flooding at the  
135 Taipingyi hydropower station located 200 m upstream.

137 Xiaojia gully, is a moderate debris flow hazard area based on limited past occurrences and has no existing  
138 engineered mitigation measures. Following a period of debris flow activity in 2010, and after a period of  
139 continuous heavy rainfall approximately  $30,000 \text{ m}^3$  of deposits were remobilised and transported along the channel  
140 to the gully mouth. This event led to a period of disruption on the S303 road from flooding (Liu et al., 2014).  
141



142  
143 **Figure 1:** Location of the three gullies that form the focus of this study within Sichuan Province. Recorded post-  
144 2008 landslide occurrences are from the Wang et al. (2022) multitemporal datasets (© Google Earth 2019).



147  
148 **Figure 2:** Schematic of our method. The key data sources comprise three multi-temporal datasets, including two  
149 from Fan et al. (2019a) covering debris flow and triggering rainfalls, as well as mitigation measures. The third  
150 dataset is adapted from Fan et al., (2019a) and highlights gully's with debris flow events post-2008 including  
151 information on the flow volume and presence of mitigation. Additional spatial data sources include aerial imagery  
152 from OpenStreetMap (OpenStreetMap contributors., 2023), World Settlement Footprint (World Settlement  
153 Footprint., 2019) and Shuttle Radar Topography Mission (SRTM) (Farr et al, 2007).  
154  
155

156 **3.1 Data Classification**  
157

158 This study builds on existing multi-temporal debris flow datasets produced by Fan et al., (2019a). Dataset 1 has  
159 an aerial extent of 892 km<sup>2</sup> and presents the location and dimensions of debris flow events between 2008 and  
160 2020. Dataset 2 presents a list of mitigative actions e.g., construction of check dams, taken between 2008–2011.  
161 We used an SRTM DEM to construct elevation profiles of Cutou, Chediguan and Xiaojia gullies to extract  
162 topographic characteristics to understand the mechanism of slope failure in the event of a rainfall-induced debris  
163 flow. These profiles facilitate morphological valley changes from debris flows to be identified. Through a  
164 comparative analysis of the 20<sup>th</sup> August 2019 debris flows in Cutou and Chediguan, we investigated the relative  
165 difference in land use change in the two gullies from 2008 to 2019, with a focus on changes before and after the  
166 2019 flow event.

167 Landscape modification from 2005 to 2019 were mapped using high resolution (0.5 to 2.5m) satellite images  
168 (Table 1). We selected images with less than 50% cloud cover and cross-referenced the mapped features with  
169 existing data sources in OpenStreetMap (OpenStreetMap contributors., 2023) and Dynamic World (Brown et al.,  
170 2022). Where satellite imagery was unavailable, we used aerial photos obtained from Google Earth,  
171 OpenStreetMap and World Settlement Footprint (World Settlement Footprint., 2019). It should be acknowledged  
172 that platforms like OpenStreetMap offer a regional view of Wenchuan rather than a detailed local-scale with  
173 mapping limited to main roads and 150 settlement polygons. However, this study's locations are unaffected by  
174 this due to their position next to the G213 national highway and G4217 road.  
175

**Table 1** Satellite and aerial imagery used for data analysis and interpretation of the built environment.

Data ID	Data Source	Acquisition Date	Resolution (m)
Aerial Satellite	Worldview (in QGIS – ‘Satellite’ XYZ tile)	2022	1.0
Satellite	Worldview (in Google Earth Pro., 2023)	10.12.2010 26.04.2011 03.04.2018 29.10.2019	1.0
Satellite	Planet	14.08.2019 24.08.2019	3.0
Satellite	Maxar Technologies (in Google Earth Pro., 2023)	09.09.2005 26.04.2011	3.0
Satellite	CNES/Airbus (in Google Earth Pro., 2023)	15.04.2015	1.0

We mapped features corresponding to human activities such as roads and properties. We highlighted at-risk zones in Cutou, Chediguan, and Xiaojia. We focus on spotlighting areas of high debris flow exposure in Cutou and Chediguan, comparing them with Xiaojia to evaluate the efficacy of check dams in mitigating potential debris flow hazards downstream of the dams.

### 3.2 Modelling Future Debris Flow Runout and Building Exposure

Both Cutou and Chediguan had check dams installed after the 2008 earthquake, while the Xiaojia gully remained unmodified. We compared the impacts of 2019 debris flows in Cutou and Chediguan gullies with a 2011 debris flow event in Xiaojia to identify the effectiveness of artificial dams in mitigating exposure to post-seismic debris flows. By using scenario modelling we identified at which point, does the size of the hazard, outweigh the mitigative capacity of the check dam to prevent overtopping. We mapped debris flows of differing scales within each of our three catchments using LAHARZ. LAHARZ is a GIS toolkit for lahar hazard mapping and modelling, developed by the USGS to calculate the area of inundation and cross sections based on empirical scaling relationships between area and volume (Schilling., 2014; Iverson et al., 1998). These empirical relationships allow for the creation of realistic inundation areas without a priori knowledge of the rheological parameters. The model simulates a debris flow triggered at a source point located on a digital elevation model and with an initial source volume. The model calculates the flow path downslope of the triggering location then generates a cross-section at each point downslope that represents the depositional volume for that area (Iverson et al., 1998).

We implemented this model using the extension in ArcGIS (Schilling., 2014). We used the 30m resolution DEM as an input, as it is the most reliable of the globally available DEMs. We identified the source areas of 2019 debris flows for Chediguan and Cutou and the 2011 for Xiaojia (Cutou – 351603, 3473449; Chediguan – 350846, 3453894; Xiaojia – 356666, 3439268) from satellite imagery and used these as the triggering locations for our simulations. We then prescribed three input volumes at each of these locations ( $10^4 m^3$ ,  $10^5 m^3$  and  $10^6 m^3$ ). The flow volumes simulate a range of observed post-2008 debris flows, representing low, high, and extreme debris flows documented in the Fan et al., (2019a) datasets. The volumes we selected reflects the range of similar hazard events in comparable geomorphological settings such as other parts of China and Italy (Wu et al., 2016; Bernard et al., 2019). For catchments with check dams, we added barriers at each check dam location by raising the cell count of the DEM by the height of the check dam obtained from field imagery.

The model was validated by comparing simulated runout extents with observed debris flows from post-2008 events. While a 30m resolution was the only available DEM for our study locations, we tested the sensitivity of DEM resolution on the extent of the final flow. A higher, 10m resolution DEM was available for the Cutou gully and we ran LAHARZ for that catchment. While the 10m DEM created a more effective flow path compared to the mapped data, the flow depositional area was similar in both the 10m and 30m scenario (RMSE 18m). Given the lack of a significant difference between the two DEM resolution we ran 30m scenarios across the three catchments. We note that there is not a strong understanding currently of what controls the maximum size of debris flows within Wenchuan catchments, hence we cannot attribute a particular probability to each scenario.

In the analysis of post-seismic debris flow, exposure and vulnerability assessments plays a crucial role (Lo et al., 2012). However, adapting traditional vulnerability methods which analyse inherent fragility and the potential loss of elements at risk, both attainable through remote practises, calculating exposure with minimal onsite data,

remains a challenge. We adapted a vulnerability model by Zou et al. (2019) to quantify the extent of exposure to the built environment at our three sites, Cutou, Chediguan and Xiaojia.

Utilising satellite and/or aerial imagery and extracting spatial characteristics to identify both elements at risk as well as hazard-affected zones, our analysis facilitates the assessment of regional exposure without relying heavily on data collected onsite. Our model quantifies the susceptibility of the built environment to debris flow damage. The degree of exposure,  $E_{df}$ , is expressed as:

$$E_{df} = E_b \times C \pm M \quad (1)$$

$E_b$  is the number of buildings damaged, and  $C$  is the fragility index of the elements at risk (Zou et al., 2019). Fragility values range from 0 to +1, with higher values indicating greater susceptibility to damage and/or failure. We assigned fragility values through using a mixture of literature and satellite images; buildings shown to be inundated or damaged in previous events or situated along the channel or gully mouth were given a value of 1, all other buildings were set a value of 0. These values were validated using historical damage reports, where available, from the 2008 earthquake recovery period to ensure applicability (Zeng et al., 2015; Wei et al., 2021; Petley et al., 2023). This approach allows for replicable application designs in similar hazard-prone areas.

The key difference between our method and that of Zou et al (2019) is the incorporation a modification factor,  $M$ , to account for the effectiveness of engineered measures like check dams in mitigating building damage and subsequent exposure. The mitigation factor,  $M$ , quantifies the influence of engineered measures, in this study check dams, on the vulnerability and subsequent exposure of buildings to debris flow impacts. The addition of this factor brings an evaluative element to the exposure assessment, quantifying the influence of check dams and assigning values ranging from -1.0 to +2.0 to reflect a spectrum of mitigation outcomes:

- $M = -1$ : Effective mitigation of debris flows, resulting in a significant reduction in hazard exposure, as evidenced by a decrease in the number of buildings damaged during historical events following construction.
- $M = 0$ : No mitigation present; exposure levels are entirely dependent on natural site conditions.
- $M = +1$ : Ineffective mitigation; there is no reduction in the number of buildings impacted in recorded debris flow events following dam construction.
- $M = +2$ : Mitigation increases exposure. Recorded events of similar volume show an increase in the number of buildings impacted following dam construction.

The above -1 to +2 scale was selected to capture a nuanced relationship between mitigation effectiveness and vulnerability. A reduction in  $M$  (e.g., -1) lowers hazard exposure by reducing flow impacts at critical locations, thereby decreasing  $E_{df}$ . Conversely, an increase in  $M$  (e.g., +2) elevates exposure, as development in hazard-prone areas amplifies the potential for damage. For example, a decrease in  $M$  by one unit (from 0 to -1) reflects an improvement in flow attenuation due to effective check dams, reducing overall exposure. Conversely, an increase in  $M$  by one unit (from 0 to +1) signifies a scenario where mitigation fails, e.g. the 2019 debris flow event in Cutou, maintaining high exposure levels. At  $M = +2$ , exposure exceeds natural vulnerability due to increased hazard presence caused by intensified land use near mitigation structures.

This scale was developed through a combination of evaluating present hazard mitigation and analysing of historical data, particularly from the 2008 earthquake recovery. Moreover, this approach, based upon the methodology proposed by Zou et al. (2019), allows for an assessment of exposure by considering both the physical resistance of buildings and the efficacy of mitigation efforts.

## 4. Results

### 4.1 Assumptions

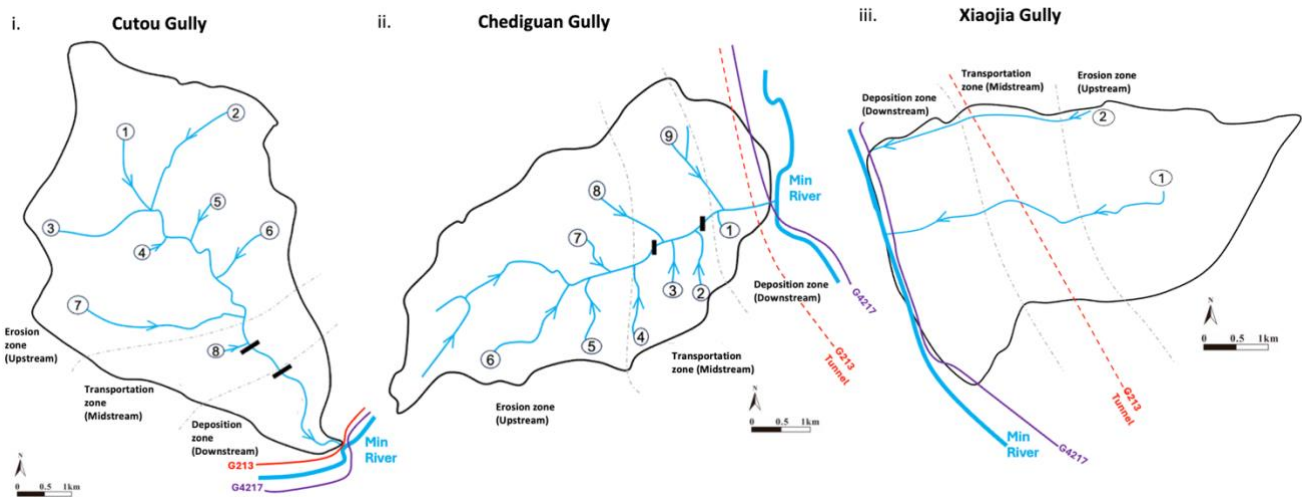
In constructing the building inventory for Cutou and Chediguan, a comprehensive approach was taken to ensure accuracy and completeness. We used aerial and satellite imagery spanning 14 years, with a focus on mapping changes from 2011 to 2019. This involved careful analysis to delineate individual buildings, considering variations in size, shape, and spatial arrangement. Mapping efforts for Xiaojia were limited to 2010-2011 due to suboptimal image quality. Our approach incorporated assumptions regarding structural categorisation, including residential, industrial, and commercial buildings. These assumptions were informed by existing literature on local building

282 typologies and architectural styles (Hao et al., 2013; Hao et al., 2012) and aerial photograph analysis from  
 283 platforms such as Google Earth and Dynamic World. By amalgamating diverse information sources, we aimed to  
 284 create a comprehensive inventory that correctly reflects the built environment of the study area.  
 285

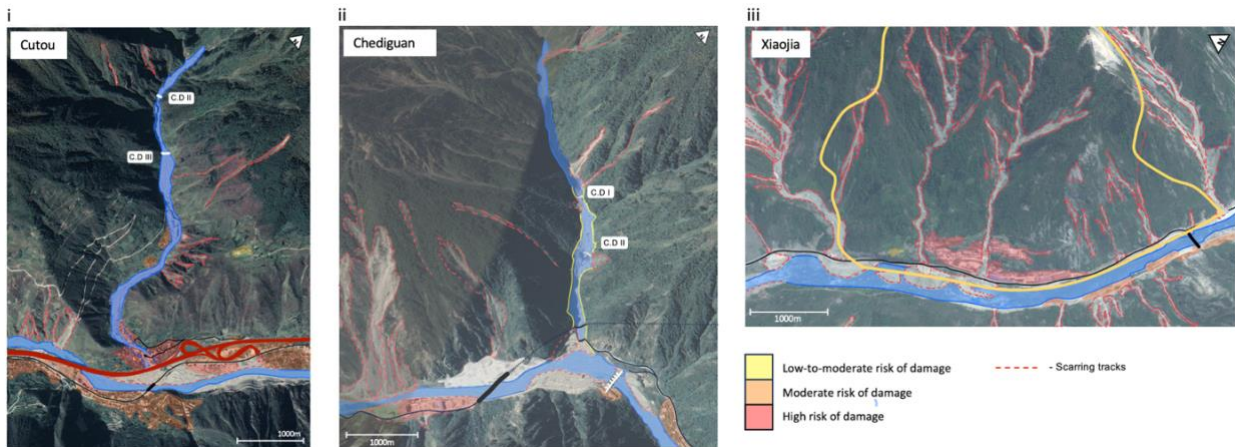
286 Additionally, we used a 30-meter Digital Elevation Model (DEM) obtained from the SRTM dataset (Farr et al.,  
 287 2007). However, it is necessary to acknowledge the limitations of this data, particularly its low resolution and  
 288 subsequent blockiness, which potentially hindered detailed topographical analysis. Despite this, the DEM  
 289 provided valuable contextual information for understanding the terrain and its influence on building distribution  
 290 and spatial patterns within the three sites. Furthermore, while using the empirical LAHARZ model for debris flow  
 291 inundation mapping, we had to account for a degree of approximation in both aerial coverage and debris flow  
 292 inundation due to the 30m resolution of the DEM file.  
 293

#### 294 4.2 Mapping Post-Earthquake Risk

295  
 296  
 297 Analysis of satellite imagery from 2005 to 2019, and topographic profiles, reveals channel widening, deepening,  
 298 aggradation, and deposition, likely attributed to the mobilisation of coseismic deposits and subsequent debris flow  
 299 occurrences (Zhang et al., 2015; Wang et al., 2018) (Fig 3). These observations allowed us to determine the zones  
 300 of erosion, transportation, and deposition for each gully and to track changes over time. Hydrological and  
 301 geomorphological analysis examines landscape morphology to identify erosional and depositional features i.e.,  
 302 scarring, changes to river channel, sediment buildup (Fig 4). By integrating the above, we delineated erosion-  
 303 prone areas, which permitted sediment transport routes to be approximated, and identify locations of sediment  
 304 deposition along the hydrological profile.



305  
 306 **Figure 3:** Hydrological profiles for the 3 study sites. Dam locations approximated for Cutou (i) and Chediguan  
 307 (ii) based on a combination satellite imagery. Streams and main tributaries are numbered. Catchment profiles have  
 308 been segmented into 3 zones – ‘erosion’, ‘transportation’ and ‘deposition’ and key infrastructure annotated.



309 **Figure 4:** Satellite images of the 3 study locations highlighting areas of scarring from previous debris flow activity  
 310 and areas of increased erosion (© Google Earth 2019). Dam locations have been approximated for Cutou (i) and  
 311 Chediguan (ii). The built environment has been shaded based upon risk of damage based upon proximity to areas  
 312 of high erosion. Critical infrastructure has been added where appropriate: black like represents the G4217 road  
 313 with the thicker sections representing bridges and the dashed lines, tunnels. The red line in (i) is the G213  
 314 Highway.  
 315

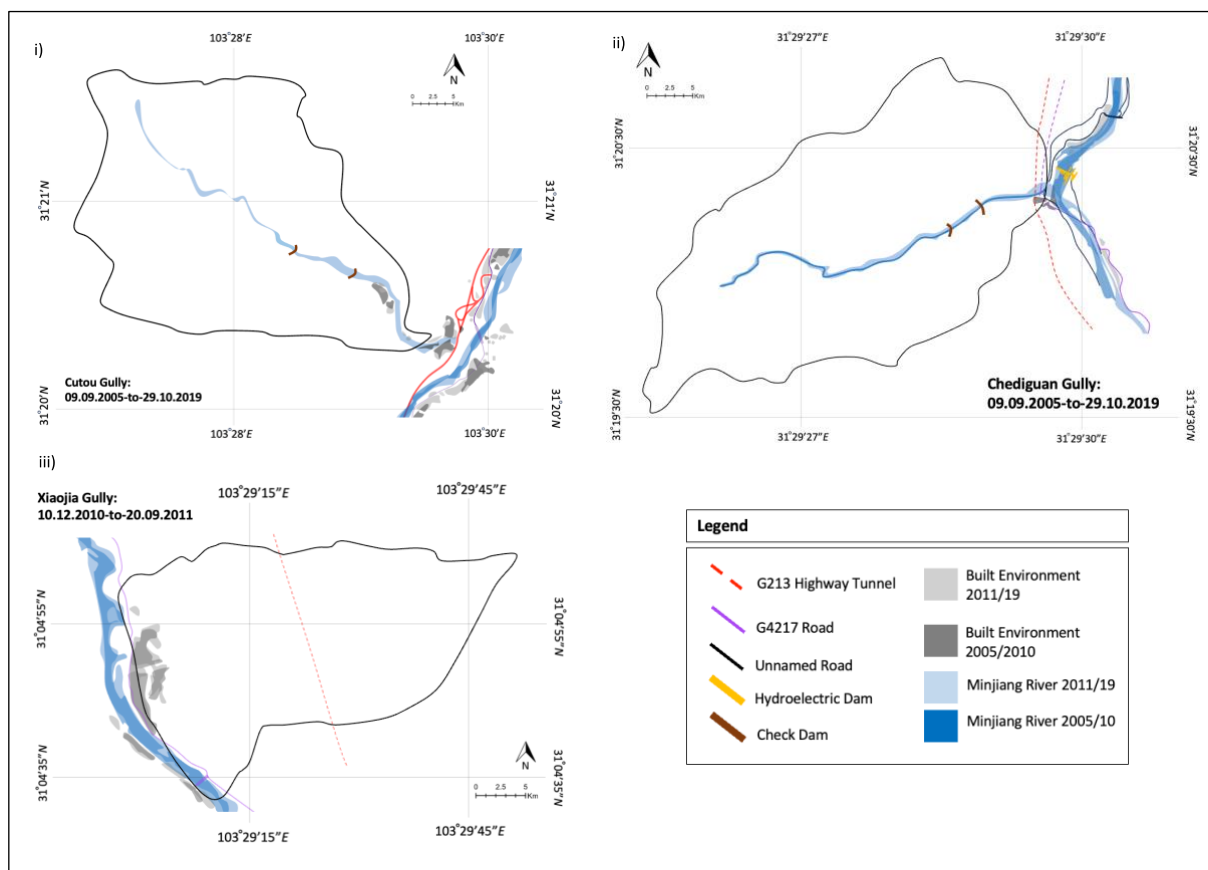
316  
 317 In Cutou and Chediguan, deposition patterns shifted post-earthquake, particularly following the construction of  
 318 check dams. Increased deposition occurs behind check dams compared to meander bends and basal slopes of the  
 319 debris fan, demonstrating the effective sediment trapping of the check dams (Wang et al., 2019). Regarding the  
 320 erosion patterns in Xiaojia, we observed common patterns in the upper gully sections at higher elevations, with  
 321 deposition occurring at the basal slopes. This is due to the absence of structural alterations to the channel,  
 322 permitting sediment to be transported to the channel and subsequent river outlet directly. The deposition patterns  
 323 in Cutou and Chediguan, are strongly controlled by the distribution of check dams, in the middle and downstream  
 324 portions of the catchment (Wang et al., 2019). The complex interplay between natural and anthropogenic factors  
 325 demonstrates the dynamic evolution of risk in post-earthquake catchments and highlights the role of check dams  
 326 in both mitigating and potentially exacerbating risk.  
 327

328 The landscape morphology prior to the 2008 earthquake was marked by extensive vegetation (over 70% of land  
 329 cover) and minimal permanent engineered features. Cutou gully contained a widespread distribution of buildings  
 330 along both the mid and lower slopes. Figure 5 shows the growth of the built environment between 2005 and 2019  
 331 in Cutou and Chediguan and between 2010 to 2011 in Xiaojia. The built environment in Cutou is concentrated  
 332 within the transportation and deposition zones on both sides on the stream. In Chediguan by comparison we  
 333 observed fewer residential structures, mostly industry and some commercial structures. Additionally, buildings in  
 334 the gully are more spread out than in Cutou highlighted by the isolated settlements to the south of the catchment  
 335 and single industrial site situated in the basin. Post-2008, noticeable tracks of scarring from debris flows are  
 336 concentrated downstream of dams 2 and 3 in Cutou (Fig 4(i)), and upstream of dams 1 and 2 in Chediguan (Fig  
 337 4(ii)). Deposition patterns are evident downstream of all modifications, forming a depositional zone,  
 338 encompassing approximately 15% and 20% of the built environment in 2019 within the transportation zone of  
 339 Cutou and Chediguan, respectively.  
 340

341 Xiaojia was chosen as the comparative catchment due to the absence of engineered mitigation such as check dams.  
 342 This analysis of Xiaojia therefore enables comparisons on the effectiveness and limitations of engineering  
 343 approaches applied to Cutou and Chediguan. In Xiaojia, the lack of engineered dam structures, results in different  
 344 erosion and deposition patterns compared to the other two catchments. Distinct patterns of upstream erosion and  
 345 downstream deposition are observed, contrasting with the more controlled environments in the modified gullies,  
 346 where deposition occurs on the northern channel flank and pronounced erosion on the southern flank. The data  
 347 availability for building types, quality and spatial distribution was limited to remote sensing images and few  
 348 literature sources, which restricts our ability to thoroughly assess how specific building characteristics, such as  
 349 materials, influence the exposure of the built environment to debris flow hazard. This is particularly evident in  
 350 Xiaojia, where more specific input data would be beneficial for understanding the role of urbanisation and  
 351 construction practices on risk levels.  
 352

353 Our analysis of Xiaojia unveils no discernible relationship between building development and heightened  
 354 exposure, particularly to residential and critical infrastructure. This lack of correlation is potentially linked to  
 355 factors beyond simple urbanisation patterns, like construction quality, building regulations, presence of natural  
 356 barriers, and effectiveness of mitigation measures. Natural terrain barriers observed in this gully including steep  
 357 slopes and rocky outcrops, could limit the extent of debris flow impacts by reducing the mobility of debris and  
 358 offering natural protection to certain areas. To fully understand this observation, further investigation into the  
 359 above variables is warranted. The absence of significant urban expansion, particularly post-earthquake in Xiaojia  
 360 may be a key factor in mitigating exposure. This area has experienced less intensive development compared to  
 361 Cutou and Chediguan, where urban expansion following the implementation of check dams potentially increased  
 362 exposure to debris flow hazards. Furthermore, the building quality in Xiaojia may play a significant role in  
 363 influencing its overall vulnerability. Without more detailed building-specific data, it is possible that buildings in  
 364 Xiaojia may be of higher structural integrity or designed to withstand environmental stressors better than those in  
 365 more developed catchments.

366  
 367 Additionally, detailed mapping of past debris flow events and their impacts on the built environment could provide  
 368 insights into the specific mechanisms influencing vulnerability in Xiaojia. By conducting a more comprehensive  
 369 analysis that considers these factors – especially in terms of land-use planning, construction standards and the role  
 370 of natural terrain features at the local scale, we can gain a better understanding of the complex interactions between  
 371 building development and exposure to natural hazards in Xiaojia. This, in turn, can inform more effective risk  
 372 management and mitigation strategies tailored to the unique characteristics of the area. Development in Xiaojia  
 373 primarily concentrates on the lower slopes (Fig 5(i) and (ii)) at the gully mouth, featuring the construction of  
 374 major roads and highways (G213 and G2417), alongside the expansion of existing residential areas. Chediguan  
 375 exhibits a less marked land cover transformation, owing to roads being directed through mountain tunnels.  
 376 Notably, development in Xiaojia mainly surges post-earthquake up to 2010, with only minor construction  
 377 activities documented thereafter (Fig 5(iii)).  
 378



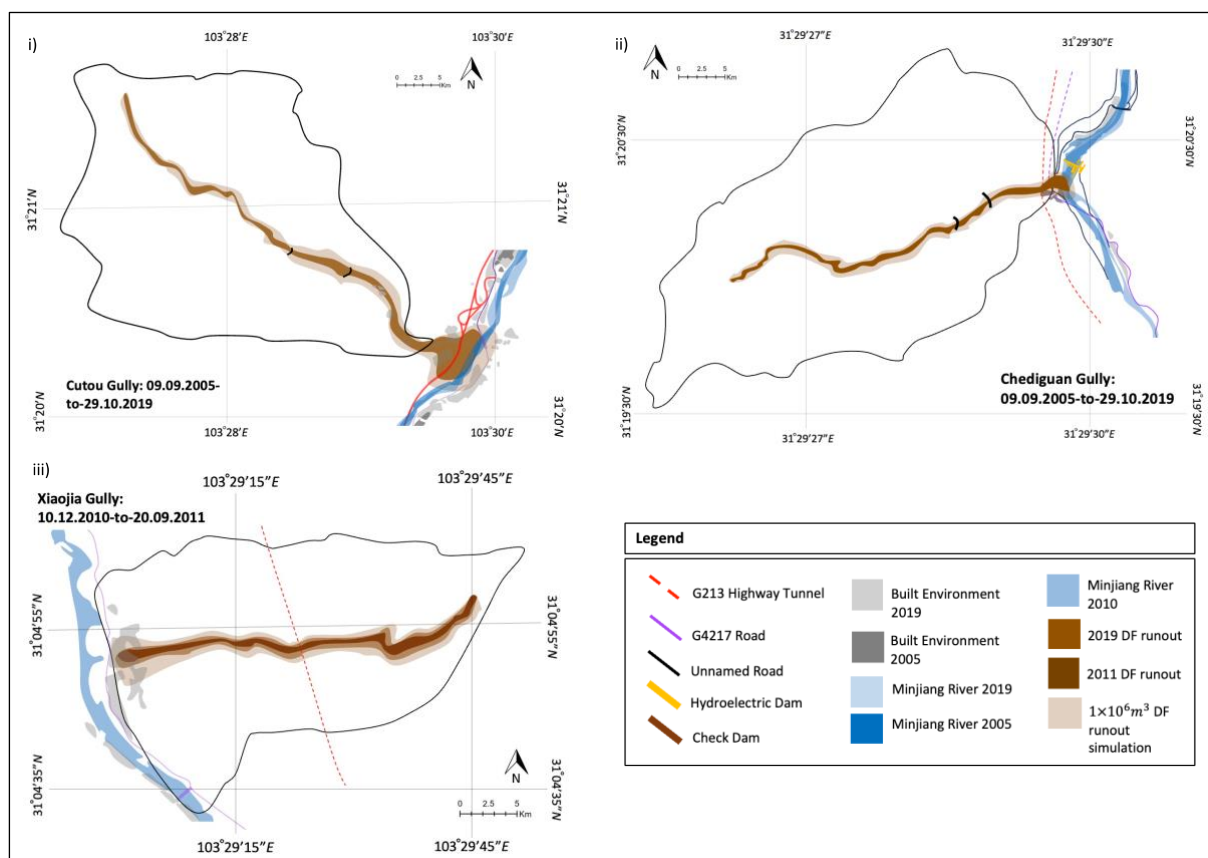
379 **Figure 5:** Evolution of the built environment and key infrastructure in (i) Cutou, (ii) Chediguan and (iii) Xiaojia  
 380 post-earthquake between 2005 and 2019.  
 381

382  
 383 We mapped the number of buildings impacted by debris flows that occurred within the Chediguan and Cutou  
 384 gullies. At 02:00 a large-scale debris flows hit Chediguan, impacting numerous structures, at around 05:00 a

385 similar debris flow hit Cutou with significant inundation noted. 79 of the 197 buildings (40%) in Cutou (Fig 5(i))  
 386 were impacted by the flow i.e., flooded, damaged, or destroyed. Buildings in Chediguan were less impacted by  
 387 that event with 7 out of the total 69 (10.1%). We combined the satellite imagery with the datasets produced by  
 388 Wang (2022) which supported our observations of check dam overtopping in both Cutou and Chediguan during  
 389 the 2019 event. In 2011 a similar event in Xiaojia impacted approximately 5 of the 43 (11.6%) buildings in the  
 390 gully (Fig 5(iii)).

### 4.3 Modelling exposure to post-earthquake debris flows

395 Our LAHARZ simulations demonstrate a clear correlation between exposure and debris flow runout, revealing a  
 396 notable increase in building damage as runout volumes escalate from low ( $10,000\text{m}^3$ ) to high ( $100,000\text{m}^3$ ) and  
 397 extreme ( $1,000,000\text{m}^3$ ) scenarios across all catchments. Despite the presence of check dams, the 2019 debris flows  
 398 recorded runout volumes significantly larger than the maximum simulated volume, resulting in substantial  
 399 building and infrastructural loss in Cutou (Fig 6(i)) and Chediguan (Fig 6(ii)).



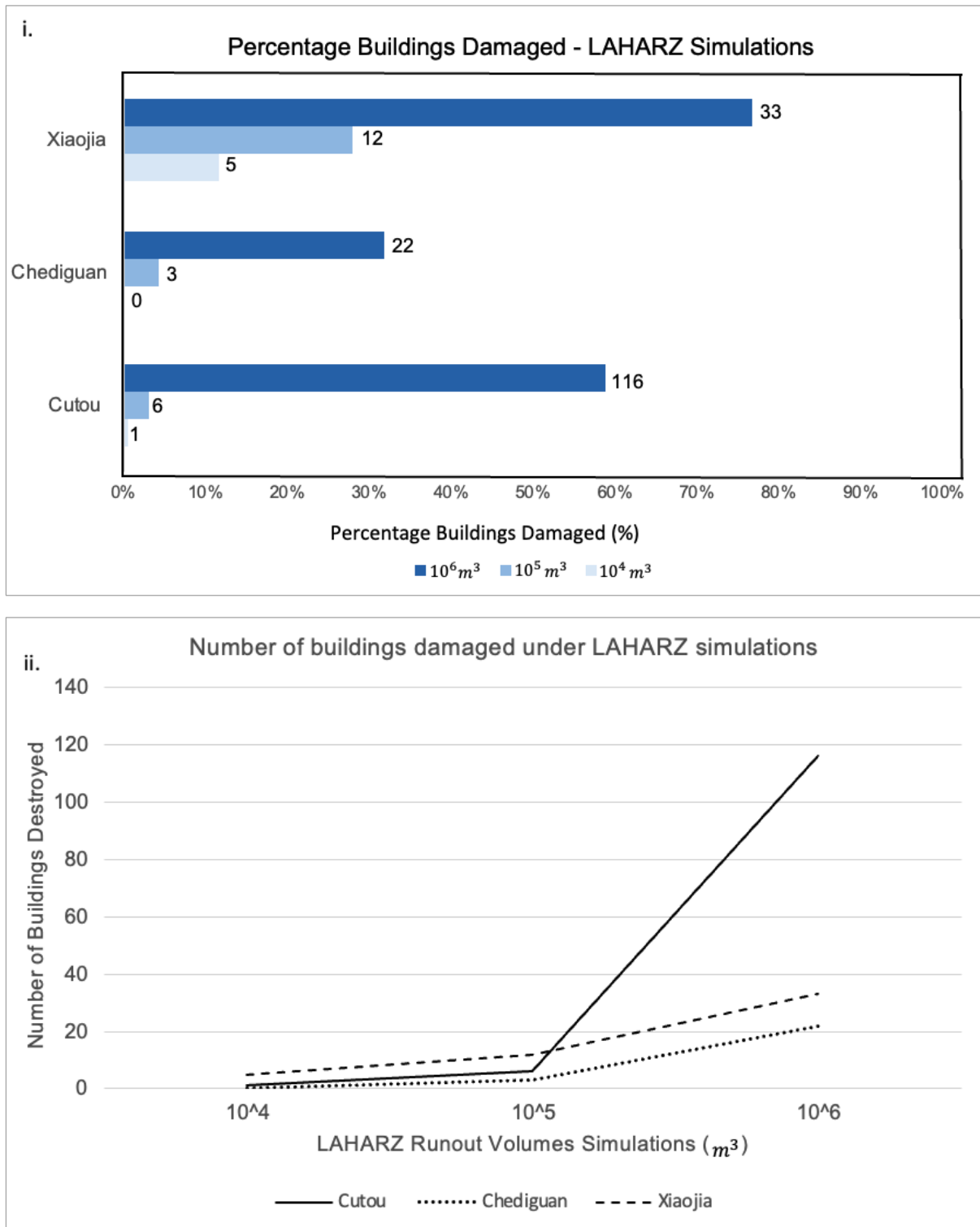
402 **Figure 6:** Debris flow runouts for 2019 in Cutou (i) and Chediguan(ii) and 2011 in Xiaojia (iii) underlain by the  
 403 extreme LAHARZ runout scenario. Low and high runouts are not displayed as they are not easy to visualise at  
 404 map scale.

407 We examined the temporal dynamics of building changes within the three gullies in response to check dam  
 408 development, while also considering the implications of the levee effect (fig 6). Our simulations revealed the  
 409 effectiveness of engineered measures in mitigating exposure to debris flow events. In both Cutou and Chediguan,  
 410 the presence of check dams led to reduced exposure at low and high debris flow volumes (fig 7(i) and (ii)).  
 411 However, the mitigative structure provides no discernible protection against extreme debris flows. Notably, Cutou  
 412 consistently exhibited elevated exposure to debris flow runout compared to Chediguan. The unengineered Xiaojia  
 413 provided an informative comparison (fig 6(iii)), highlighting the effectiveness of check dams at low and high  
 414 debris flow volumes. Xiaojia's post-2011 expansion appeared restrained, indicating a potential adaptive response  
 415 following debris flow events. In contrast, substantial expansion occurred in Cutou and Chediguan between 2011

416 and 2019, despite experiencing a debris flow event in 2013, suggesting the impact of check dams implemented  
417 post-2013.

418  
419 Furthermore, the incremental increase between high and extreme simulations in Xiaojia paralleled Chediguan's  
420 gradual incline, diverging from Cutou's steep escalation. Xiaojia sustained a maximum building damage of 33%  
421 under extreme scenarios, compared with 59% in Cutou and 22% in Chediguan. This discrepancy suggests that the  
422 optimal efficiency of check dams may be surpassed, urging consideration of additional factors such as the  
423 landscape's inherent resilience. Our observations underscore the nuanced variability in the effectiveness of check  
424 dams, influenced by contextual factors and landscape characteristics.

425  
426  
427  
428  
429  
430  
431  
432  
433  
434  
435  
436  
437  
438  
439  
440  
441  
442  
443  
444  
445  
446  
447  
448  
449  
450  
451  
452



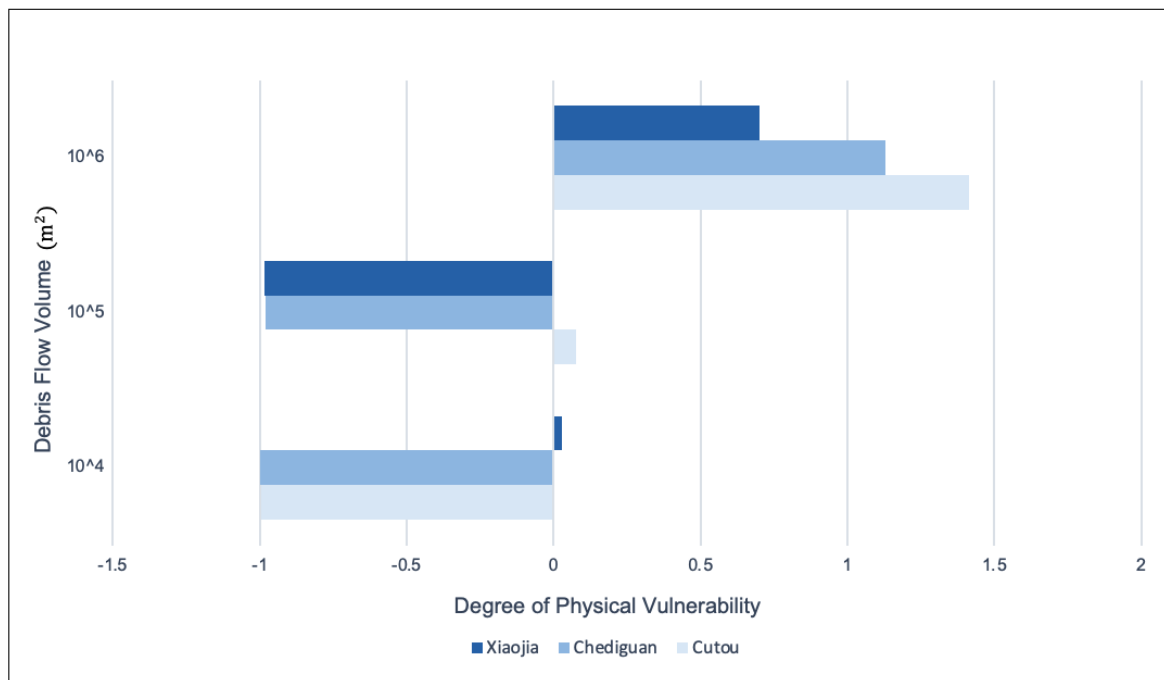
454 **Figure 7:** Built environment impacts from three debris flow scenarios modelled using LAHARZ at Cutou,  
 455 Chediguan and Xiaojia. (i). Percentage of buildings damaged as a proportion of total buildings (Cutou – 197,  
 456 Chediguan – 69 and Xiaojia – 43) in each scenario. The numbers at the end of the bars are the number of buildings  
 457 damaged buildings in that debris flow scenario. (ii) Total number of buildings damaged by each simulated debris  
 458 flow.

459  
 460

461 Figure 7 illustrates how a tenfold increase in runout volume corresponds to building damage, with a discernible  
 462 rise in impacted building numbers noted between low and high scenarios, and a significant incline between high

463 and extreme scenarios across all catchments. These simulations provide valuable insights into the efficacy of  
 464 engineered mitigation structures. While check dams in Cutou and Chediguan effectively reduce exposure at low  
 465 and high runout volumes, concerns arise when surpassing the maximum capacity. Urbanisation emerges as a  
 466 significant contributing factor impacting exposure and future risk, with the presence of check dams during the  
 467 2019 events significantly contributing to the built environment's exposure. However, due to the lack of available  
 468 data on building materials in these three regions, we were unable to quantify their influence on structural  
 469 vulnerability. As a result, exposure was determined to be the primary contributing factor to building damage. To  
 470 fully understand the effect of check dams and validate our statistical approach, comprehensive numerical analysis  
 471 of multiple hazard events in each gully is necessary. This sub-section addresses the elements driving hazard-  
 472 related risk scenarios, including the trigger event, return period, and level of damage, and underscores the  
 473 importance of considering these factors when suggesting and implementing modifications.

475 The exposure model is applied to historical events (2019 and 2011) and LAHARZ simulations, showcasing  
 476 changes in the degree of exposure across the catchments with increasing debris flow runout volumes (Fig 8).  
 477 Consistent with earlier observations in exposure, Cutou exhibits a heightened vulnerability to debris flows at 64%  
 478 after the 2019 event, followed by Chediguan at 52% and Xiaojia with 2% in 2011. A discernible change in building  
 479 exposure is observed between the high and extreme scenarios across all catchments. The most influential factor  
 480 in overall vulnerability remains the number of buildings, highlighting urbanization as a contributing factor  
 481 impacting both exposure and physical vulnerability. Moreover, the presence of failed check dams in Cutou and  
 482 Chediguan during the 2019 events significantly contributes to their physical vulnerability.



483 **Figure 8:** Changes in the degree of exposure with increasing runout volumes using the exposure model developed  
 484 in equation 1. The 2011 and 2019 debris flows are also noted as a base marker from an observed hazard event.  
 485

486  
 487 **5. Discussion**

488 Post-earthquake structural interventions influence the volume and spatial distribution of sediment within the  
 489 catchment. Our observations show that check dams act as local depocentres within the catchment, often storing  
 490 large volumes of sediment upstream of the majority of building development. The choices made about post-  
 491 earthquake development of the built environment, particularly housing, and mitigative measures like check dams,  
 492 evolve rapidly without a clear approach to mitigating adverse long-term consequences of sediment retention  
 493 behind dams (McGuire et al., 2017). Additionally, the processes driving geological disasters in the complex  
 494 landscape of the Longmenshan occur at different timescales to the rapid socio-economic development in the region  
 495 (Chen et al., 2022).

496  
 497 Although our analysis focuses on smaller-scale communities, the implications drawn from our findings echo those  
 498 of broader studies. For instance, Arrogante-Funes et al. (2021)'s extensive investigation into hazard mitigation

499 strategies in larger geographical regions, drew parallels to the effectiveness and limitations of mitigation measures  
500 to debris flows. Similarly, Chen et al. (2021) provided insights into the complexities of hazard mitigation,  
501 emphasising the necessity of adaptive responses considering local contexts. This aligns with our analysis that each  
502 gully must be assessed and mitigated individually rather than collectively to account for local geological and  
503 hydrological influences on mitigation effectiveness. Moreover, Li et al. (2018) examined the long-term impact of  
504 engineering interventions, noting the variability in check dams effectiveness over time. This supports our  
505 conclusion that the diminishing effectiveness of check dams is likely the result of sediment accumulation and  
506 structural degradation and highlights the necessity for their continued maintenance post-construction in addition  
507 to adaptive mitigation strategies. Furthermore, Eidsvig et al. (2014) and Tang et al. (2011) explored the interplay  
508 between socio-economic factors and hazard vulnerability, emphasising that community resilience is directly  
509 linked to economic resource availability and social cohesion. This corroborates our understanding that debris flow  
510 mitigation is a multifaceted issue, and socio-economic conditions are integral to their success. By situating our  
511 findings within the broader context delineated by these studies, we accentuate the relevance and applicability of  
512 our research beyond the confines of the specific communities under study.

513  
514 Open check dams, similar to those established in Cutou and Chediguan, play a pivotal role in bed stabilization,  
515 slope reduction, and the regulation of sediment transport (Bernard et al., 2019). However, inadequate  
516 understanding of post-earthquake debris flow characteristics has led to the failure of many newly constructed  
517 engineered structures to mitigate hazards effectively, amplifying damage instead (Chang et al., 2022). During the  
518 August 2019 debris flow, Cutou experienced the highest inundation, with 40% of surveyed structures directly  
519 affected, including critical infrastructure like the G4217 highway bridge. In Chediguan, despite a declined  
520 industrial presence, debris flow impacts affected 7% of structures. The presence of check dams in both locations  
521 contributed to raised exposure and hazard impacts during the 2019 event, with overtopping and damage to dam  
522 sections recorded.

523  
524 We conducted LAHARZ scenarios to predict potential exposure to debris flows with volumes that have been  
525 observed within the catchments and the region. Our results highlighted a clear correlation between exposure and  
526 debris flow runout, showing notable increases in building damage as runout volumes escalated from low to  
527 extreme across all catchments. We observed two key elements to the role of check dams in affecting exposure to  
528 debris flows. When empty, check dams are effective at mitigating the effects of small and medium volume debris  
529 flows. Yet, they are not effective at mitigating the largest of debris flows observed in this region. Large runout  
530 volumes in the 2019 debris flows resulted in substantial building and infrastructural loss in both Cutou and  
531 Chediguan, suggesting a negative contribution from damaged check dams. Cutou was found to be highly exposed  
532 to extreme debris flow volumes, a result of its raised development level situated at the basal slopes. The fact that  
533 Xiaojia was found to possess the least exposure to the most extreme debris flow volume suggests that there may  
534 be an adaptive component to debris flow mitigation in catchments without significant check dam development.  
535 These findings suggest that urban development and debris flow risk co-evolve based on the nature of the structural  
536 interventions the studied areas.

537  
538 Our analysis of erosion, transportation, and deposition zones for each gully revealed significant changes in  
539 landscape morphology post-earthquake, likely attributed to mobilised coseismic deposits and subsequent debris  
540 flow occurrences. The presence of check dams influenced deposition patterns, with mid-to-downstream trends  
541 indicating effective sediment retention in Cutou and Chediguan, while Xiaojia exhibited typical erosion-  
542 deposition behaviour. Our findings can be supported by a similar occurrence during the “8.13” debris flow event  
543 in Wenjiagou. The damage and subsequent failure of mitigative check dams led to the inundation of 490 houses  
544 or more recently, a debris flow in the Miansi and Weizhou townships on 27 June 2023 blocked the valley in the  
545 first instance before breaching the dam and causing 7 fatalities (Petley., 2023). Further research is thus imperative  
546 to devise appropriate mitigation approaches for post-seismic debris flows. Whilst existing literature has  
547 underscored the physical effectiveness of check dams in reducing exposure to debris flow impacts within Alpine  
548 terrains (Piton et al., 2016), it should be noted that their primary function extends beyond this to also provide  
549 socio- economic and political reassurance (Wu et al., 2012; Chen et al., 2022)

550  
551 The findings of our paper support the theory of the levee effect by demonstrating how the implementation of  
552 mitigative measures, such as check dams, can inadvertently increase exposure levels and risk perception in hazard-  
553 prone areas. The interplay between engineering solutions and the built environment as highlighted in our study  
554 through analysis of the 2011 and 2019 events as well as the LAHARZ simulations, illustrates the levee effect.  
555 Similar to previous studies on flooding and the levee effect. Similar to previous studies on flooding, (e.g.  
556 Collenteur et al., 2015), our paper suggests that the perceived reduction in hazard risk due to mitigative structures  
557 can lead to increased levels of exposure due to raised development in debris flow-prone regions. This effect is  
558 particularly evident in the Cutou catchment where urban expansion occurred post-dam construction, despite the

559 repeated occurrence of high magnitude debris flows. This suggests a distorted perception of hazard risk, which  
560 ultimately drives urbanisation into vulnerable areas (Chen et al., 2015; Ao et al.,2020).

561  
562 The levee effect can influence exposure to large-scale debris flow events by inadvertently increasing risk in areas  
563 protected by engineered mitigation structures, such as check dams. This occurs because the perceived safety  
564 provided by these structures can encourage development in vulnerable areas, which might otherwise remain  
565 uninhabited due to their high-risk nature. This phenomenon is best evidenced in our paper by the Cutou catchment,  
566 where the construction of check dams in 2013 coincided with widespread urban expansion, despite ongoing small-  
567 scale debris flow activity in the area. Subsequently, building exposure increased by 64% post-2008, underscoring  
568 the risk amplification associated with structural mitigation. This observation highlights the necessity of coupling  
569 structural interventions with strategies that address residual risks and foster community awareness of long-term  
570 hazard vulnerabilities. The 2019 debris flow event exemplified the risks associated with this effect, as the flow  
571 overtopped the check dams and used the stored material as a secondary fuel, significantly amplifying the impact.  
572 As a result, 40% of surveyed buildings were inundated, demonstrating how the levee effect can potentially  
573 escalate exposure to large-scale debris flow events.

574  
575 Our LAHARZ simulations further reinforce the limitations of engineered structures as the sole mitigative measure  
576 in alpine environments; urbanisation of mountainous terrains further complicates the balance between  
577 technological advancements and geological hazards (Zhang, S et al., 2014; Zhang and Li., 2020; Luo et al., 2023).  
578 Despite the presence of check dams, our extreme runout volume resulted in significant impacts on the built  
579 environment in Cutou and Chediguan, including overtopping and dam failure. The use of these simulations  
580 emphasises the challenges of reducing exposure to at-risk structures and highlights the unpredictable nature of  
581 debris flow occurrences. Moreover, our findings relating to the altered patterns of erosion and deposition  
582 emphasise the relationship between natural topography, engineered interventions, and risk perception in post-  
583 seismic debris flows. Urbanisation exacerbates this complexity, influencing exposure and physical vulnerability  
584 through deposit remobilisation. Our LAHARZ simulations serve as a practical demonstration of the levee effect,  
585 illustrating how engineered structures may not provide adequate protection against runout volumes similar to the  
586 extreme simulation, thereby reinforcing the importance of considering the levee effect in debris flow risk  
587 management. The unpredictable nature of debris flow occurrences from pinpointing their location and timing to  
588 ascertaining their volume and velocity ultimately means that the concept of the ‘levee effect’ remains core to the  
589 issue of debris flows in post-seismic Sichuan (Cucchiari et al., 2019a; Tang et al., 2022).

590  
591 Whilst our findings are not able to definitively determine the prevalence of the levee effect with regards to  
592 development in post-seismic environments like Sichuan, we hypothesise that the implementation of mitigative  
593 structures like check dams may inadvertently increase exposure levels to large-scale debris flow events by creating  
594 a false sense of safety. Although our investigation does not fully explore this phenomenon, our outcomes suggest  
595 that the development of infrastructure in areas perceived to be safe due to the presence of engineered structures  
596 may amplify hazard exposure. This highlights the limitations of solely relying on engineered interventions in  
597 reducing exposure to at-risk structures under the extreme LAHARZ scenario. Furthermore, we highlighted the  
598 complex interplay between engineering solutions and human behaviour, warranting further investigation  
599 (Papathoma-Köhle et al., 2011; Gong et al., 2021). By emphasising the challenges and limitations of engineered  
600 structures in mitigating debris flow impacts, we underscore the need for comprehensive risk management  
601 strategies that consider the complexities of urbanization and flow-based hazards in mountainous terrains.

602  
603 Despite the presence of these engineered interventions, our analysis demonstrates significant exposure levels and  
604 infrastructure damage during extreme debris flow events. This discrepancy between perceived risk reduction and  
605 actual hazard exposure underscores the need for a more comprehensive understanding of risk perception in the  
606 context of hazard mitigation strategies. Moreover, our study highlights the importance of considering human  
607 behaviour and decision-making processes in the design and implementation of risk management measures. Future  
608 research should focus on elucidating the mechanisms driving risk perception in hazard-prone areas and developing  
609 strategies to bridge the gap between perceived and actual risk to enhance the effectiveness of mitigation efforts.

## 610 611 612 **6. Conclusion**

613 Our study investigated the changing exposure to debris flows in Cutou Chediguan and Xiaojia since the 2008  
614 Wenchuan earthquake. We used high resolution satellite imagery to build a time series of building inventories  
615 between 2005 and 2019. Despite recurrent debris flow occurrences between 2010 to 2013, we observed increased  
616 urban developments across all three gullies to varying extents until 2015.

617

618 We identified significant differences in the impacts of debris flow events in 2011 and 2019 respectively. In the  
619 August 2019 debris flow, Cutou experienced the highest inundation, with 40% of surveyed structures directly  
620 affected, including critical infrastructure such as the G4217 highway bridge. In contrast, the 2011 event in Xiaojia  
621 impacted approximately 11.6% of buildings in the gully, indicating a lower level of damage compared to Cutou.  
622 The presence of check dams in Cutou and Chediguan contributed to increased exposure and hazard impacts during  
623 the 2019 event, with overtopping and damage to dam sections recorded at both locations. However, despite the  
624 presence of these mitigative structures, the impact on the built environment was significant, suggesting limitations  
625 in their effectiveness, particularly during extreme runout volumes. Our Laharz simulations demonstrated a clear  
626 correlation between exposure and debris flow runout, revealing a notable increase in building damage as runout  
627 volumes increased from low to high and finally extreme scenarios across all catchments. Despite the presence of  
628 check dams, the simulations indicated that these structures were unable to reduce the impacts on the built  
629 environment, especially during extreme events. Furthermore, our analysis highlighted a heightened level of built  
630 environment exposure in Cutou compared to Chediguan and Xiaojia driven by urbanisation, the presence of  
631 critical infrastructure, and the effectiveness of mitigative measures.

632  
633 Our findings suggest that the presence and location of check dam in gully channels likely increased building  
634 exposure and contributed to a levee effect. This raises concerns about the long-term implications, including  
635 structural integrity, maintenance and clearing. LAHARZ modelling provides comprehension of check dam  
636 efficacy, raising concerns for Cutou and Chediguan in high-to-extreme runout events. Further, the combined use  
637 of the LAHARZ GIS toolkit and exposure analysis contributes to a holistic understanding of the risk landscape,  
638 informing strategies for enhanced disaster resilience and sustainable development in vulnerable areas.

639  
640 The assumptions and subsequent considerations highlighted throughout our study underscore the complexities of  
641 how check dams, as a mitigative structure, influences land-use planning and development in hazard-prone areas.  
642 These factors ensure that the data outputs are comprehensive but also reflective of the inherent complexities of  
643 the study area and limitations in available data sources and analytical tools. We have highlighted a relationship  
644 between the presence of engineered measures like check dams alongside the built environment, showing how this  
645 relationship has contributed to increased debris flow impacts post-2008 earthquake in Sichuan, particularly  
646 provinces along the Minjiang. Our results emphasise the need for a multi-faceted approach to risk management,  
647 integrating socio-economic development and addressing the paradoxical role of mitigative structures in shaping  
648 public perception to hazard exposure and vulnerability. Understanding these complexities is vital for informed  
649 decision-making and effective debris flow risk management.

650  
651 Overall, our findings have indicated that the 2019 debris flow events caused more significant damage and higher  
652 exposure levels compared to the 2011 flow, emphasising the need for comprehensive risk management strategies  
653 in debris flow-prone areas.

#### 654 **Acknowledgements**

655 EH is supported by the BGS-NERC National Capability grant ‘Geosciences to tackle Global Environmental  
656 Challenges’ (NERC reference NE/X006255/1) and publishes with permission from the Executive Director of the  
657 British Geological Survey.

#### 658 **References**

659  
660  
661 Ao, Y., Huang, K., Wang, Y., Wang, Q. and Martek, I. 2020. Influence of built environment and risk  
662 perception on seismic evacuation behavior: Evidence from rural areas affected by Wenchuan  
663 earthquake. *International journal of disaster risk reduction: IJDRR* 46(101504), p. 101504. Available at:  
664 <https://www.sciencedirect.com/science/article/pii/S2212420919313500>.

665  
666 Arrogante-Funes, P., Bruzón, A.G., Arrogante-Funes, F., Ramos-Bernal, R.N. and Vázquez-Jiménez, R.  
667 2021. Integration of vulnerability and hazard factors for landslide risk assessment. *International journal of*  
668 *environmental research and public health* 18(22), p. 11987. Available at:  
669 <http://dx.doi.org/10.3390/ijerph182211987>.

670  
671 Bernard, M., Boreggio, M., Degetto, M. and Gregoretti, C. 2019. Model-based approach for design and  
672 performance evaluation of works controlling stony debris flows with an application to a case study at Rovina di  
673 Cancia (Venetian Dolomites, Northeast Italy). *The Science of the total environment* 688, pp. 1373–1388.  
674 Available at: <https://www.sciencedirect.com/science/article/pii/S0048969719325288>.

675  
676 Brown, C. F. *et al.* Dynamic world, near real-time global 10 m land use land cover mapping. *Scientific Data* 9,  
677 251 (2022)

678  
679 Chang, M., Luo, C., Wu, B. and Xiang, L. 2022. Catastrophe process of outburst debris flow triggered by the  
680 landslide dam failure. *Journal of hydrology* 609(127729), p. 127729. Available at:  
681 <https://www.sciencedirect.com/science/article/pii/S0022169422003043>.  
682  
683 Chen, N.-S., Hu, G.-S., Deng, M.-F., Zhou, W., Yang, C.-L., Han, D. and Deng, J.-H. 2011. Impact of  
684 earthquake on debris flows — a case study on the Wenchuan earthquake. *Journal of earthquake and*  
685 *tsunami* 05(05), pp. 493–508. Available at: <http://dx.doi.org/10.1142/s1793431111001212>.  
686  
687 Chen, X., Cui, P., You, Y., Chen, J. and Li, D. 2015. Engineering measures for debris flow hazard mitigation  
688 in the Wenchuan earthquake area. *Engineering geology* 194, pp. 73–85. Available at:  
689 <https://www.sciencedirect.com/science/article/pii/S0013795214002579>.  
690  
691 Chen, M. et al. 2021. Quantitative assessment of physical fragility of buildings to the debris flow on 20 August  
692 2019 in the Cutou gully, Wenchuan, southwestern China. *Engineering geology* 293(106319), p. 106319.  
693 Available at: <https://www.sciencedirect.com/science/article/pii/S0013795221003306>  
694  
695 Chen, Y., Song, J., Zhong, S., Liu, Z. and Gao, W. 2022. Effect of destructive earthquake on the population-  
696 economy-space urbanization at county level—a case study on Dujiangyan county, China. *Sustainable cities and*  
697 *society* 76(103345), p. 103345. Available at: <http://dx.doi.org/10.1016/j.scs.2021.103345>.  
698  
699 Collenteur, R. A., de Moel, H., Jongman, B., & Di Baldassarre, G. (2015). The failed-levee effect: Do societies  
700 learn from flood disasters? *Natural Hazards (Dordrecht, Netherlands)*, 76(1), 373–388.  
701 <https://doi.org/10.1007/s11069-014-1496-6>  
702  
703 Costa, J.E. 1984. Physical geomorphology of debris flows. In: *Developments and Applications of*  
704 *Geomorphology*. Berlin, Heidelberg: Springer Berlin Heidelberg, pp. 268–269. Available at:  
705 [http://dx.doi.org/10.1007/978-3-642-69759-3\\_9](http://dx.doi.org/10.1007/978-3-642-69759-3_9).  
706  
707 Couvert, B., Lefebvre, B., Lefort, P., & Morin, E. (1991). Etude générale sur les seuils de correction  
708 torrentielle et les plages de dépôts. *Houille Blanche*, 77(6), 449–456. <https://doi.org/10.1051/lhb/1991043>  
709  
710 Cruden, D.M. and Varnes, D.J. 1996. Landslides: Investigation and Mitigation. Chapter 3—Landslide Types  
711 and Processes. Transportation research board special report, 247. In: *Transportation research board special*  
712 *report (247)*.  
713  
714 Cucchiario, S. et al. 2019a. Geomorphic effectiveness of check dams in a debris-flow catchment using multi-  
715 temporal topographic surveys. *Catena* 174, pp. 73–83. Available at:  
716 <https://www.sciencedirect.com/science/article/pii/S0341816218304910>.  
717  
718 Cucchiario, S., Cazorzi, F., Marchi, L., Crema, S., Beinat, A. and Cavalli, M. 2019b. Multi-temporal analysis of  
719 the role of check dams in a debris-flow channel: Linking structural and functional  
720 connectivity. *Geomorphology (Amsterdam, Netherlands)* 345(106844), p. 106844. Available at:  
721 <https://www.sciencedirect.com/science/article/pii/S0169555X1930323X>.  
722  
723 Cui, P., Wei, F. Q., He, S. M., You, Y., Chen, X. Q., Li, Z. L., et al. (2008). Mountain Disasters Induced by the  
724 Earthquake of May 12 in Wenchuan and the Disasters Mitigation. *J. Mountain Sci.* 26 (3), 280–282.  
725 doi:10.35123/geo-expo\_2017\_4  
726  
727 Dai, Z., Huang, Y., Cheng, H. and Xu, Q. 2017. SPH model for fluid–structure interaction and its application to  
728 debris flow impact estimation. *Landslides* 14(3), pp. 917–928. Available at: [http://dx.doi.org/10.1007/s10346-](http://dx.doi.org/10.1007/s10346-016-0777-4)  
729 [016-0777-4](http://dx.doi.org/10.1007/s10346-016-0777-4).  
730  
731 Eidsvig, U.M.K., Papathoma-Köhle, M., Du, J., Glade, T. and Vangelsten, B.V. 2014. Quantification of model  
732 uncertainty in debris flow vulnerability assessment. *Engineering geology* 181, pp. 15–26. Available at:  
733 <https://www.sciencedirect.com/science/article/pii/S0013795214002051>.  
734  
735 Fan, X. et al. 2018. What we have learned from the 2008 Wenchuan Earthquake and its aftermath. A decade of  
736 research and challenges. *Engineering geology* 241, pp. 25–32. Available at:  
737 <https://www.sciencedirect.com/science/article/pii/S0013795218307233>.

738  
739 Fan, X., Scaringi, G., Domènech, G., Yang, F., Guo, X., Dai, L., He, C., Xu, Q., and Huang, R. 2019a. Two  
740 multi-temporal datasets that track the enhanced landsliding after the 2008 Wenchuan earthquake, *Earth Syst.*  
741 *Sci. Data*, 11, 35–55, <https://doi.org/10.5194/essd-11-35-2019>  
742  
743 Fan, X., Scaringi, G., Korup, O., West, A. J., van Westen, C. J., Tanyas, H., Niels Hovius, Tristram C. Hales,  
744 Randall W. Jibson, Kate E. Allstadt, Limin Zhang, Stephen G. Evans, Chong Xu<sup>10</sup>, Gen Li<sup>4</sup>, Xiangjun Pei,  
745 Qiang Xu<sup>1</sup>, and Runqiu Huang. 2019b. Earthquake-induced chains of geologic hazards: Patterns, mechanisms,  
746 and impacts. *Reviews of Geophysics*, 57, 421–503. <https://doi.org/10.1029/2018RG000626>  
747  
748 Farr, T. G., et al. (2007), The Shuttle Radar Topography Mission, *Rev. Geophys.*, 45, RG2004,  
749 doi:10.1029/2005RG000183.  
750  
751 Fell, R., Corominas, J., Bonnard, C., Cascini, L., Leroi, E., & Savage, W. Z. 2008. Guidelines for landslide  
752 susceptibility, hazard, and risk zoning for land use planning. *Engineering Geology*, 102(3–4), 85–98.  
753 <https://doi.org/10.1016/j.enggeo.2008.03.022>  
754  
755 Francis, O. Fan, X., Hales, T., Hobbey, D., Xu, Q., Huang, R (2022) ‘The fate of sediment after a large  
756 earthquake’, *Journal of Geophysical Research: Earth Surface*, 127(3). doi:10.1029/2021jf006352  
757  
758 Gong, X.-L., Chen, X.-Q., Chen, K.-T., Zhao, W.-Y. and Chen, J.-G. 2021. Engineering planning method and  
759 control modes for debris flow disasters in scenic areas. *Frontiers in earth science* 9. Available at:  
760 <http://dx.doi.org/10.3389/feart.2021.712403>  
761  
762 Google Earth Pro. Version 9.189.0.0 “Location of Cutou gully, Chediguan Gully and Xiaojia Gully,  
763 Sichuan, China”. Image taken 2020. Accessed June 2, 2023.  
764  
765 Guo, X., Cui, P., Li, Y., Ma, L., Ge, Y., and Mahoney, W.B. 2016. Intensity–duration threshold of rainfall-  
766 triggered debris flows in the Wenchuan Earthquake affected area, China. *Geomorphology* (Amsterdam,  
767 Netherlands) 253, pp. 208–216. Available at: <http://dx.doi.org/10.1016/j.geomorph.2015.10.009>.  
768  
769 Guzzetti, F. et al. 2008. The rainfall intensity-duration control of shallow landslides and debris flows: An  
770 update. *Landslides* 5(1), pp. 3–17. [Doi: 10.1007/s10346-007-0112-1](https://doi.org/10.1007/s10346-007-0112-1).  
771  
772 Hao, P. Hooimeijer, P. Sliuzas, R and Geertma, S. 2013 ‘What drives the spatial development of urban villages  
773 in China?’, *Urban Studies*, 50(16), pp. 3394–3411. doi:10.1177/0042098013484534  
774  
775 Hao, P. (2012) *Spatial evolution of urban villages in Shenzhen*. dissertation. University of Utrecht. Available at:  
776 [https://webapps.itc.utwente.nl/librarywww/papers\\_2012/phd/puhao.pdf](https://webapps.itc.utwente.nl/librarywww/papers_2012/phd/puhao.pdf)  
777  
778 He, N., Fu, Q., Zhong, W., Yang, Z., Cai, X. and Xu, L. 2022. Analysis of the formation mechanism of debris  
779 flows after earthquakes – A case study of the Legugou debris flow. *Frontiers in ecology and evolution* 10.  
780 Available at: <http://dx.doi.org/10.3389/fevo.2022.1053687>  
781  
782 Horton, A.J. et al. (2019) ‘Identifying post-earthquake debris flow hazard using Massflowx’, *Engineering*  
783 *Geology*, 258, p. 105134. doi:10.1016/j.enggeo.2019.05.011  
784  
785 Hu, K.H., Cui, P., and Zhang, J.Q. 2012. Characteristics of damage to buildings by debris flows on 7 August  
786 2010 in Zhouqu, Western China. *Natural hazards and earth system sciences* 12(7), pp. 2209–2217. Available  
787 at: <https://nhess.copernicus.org/articles/12/2209/2012/nhess-12-2209-2012.pdf>.  
788  
789 Huang, R. Q., & Li, W. L. 2009. Analysis of the geo-hazards triggered by the 12 May 2008 Wenchuan  
790 Earthquake, China. *Bulletin of Engineering Geology and the Environment*, 68(3), 363–371.  
791 <https://doi.org/10.1007/s10064-009-0207-0>  
792  
793 Huang, R., Pei, X., Fan, X., Zhang, W., Li, S. and Li, B. 2012. The characteristics and failure mechanism of  
794 the largest landslide triggered by the Wenchuan earthquake, May 12, 2008, China. *Landslides* 9(1), pp. 131–  
795 142. Available at: <http://dx.doi.org/10.1007/s10346-011-0276-6>.

- 786  
787 Huang, R. and Li, W. 2014. Post-earthquake landsliding and long-term impacts in the Wenchuan earthquake  
788 area, China. *Engineering geology* 182, pp. 111–120. Available at:  
789 <http://dx.doi.org/10.1016/j.enggeo.2014.07.008>.  
790
- 791 Hübl, J. and Fiebiger, G. 2005. Chap. 18 - Debris-flow mitigation measures. In: *Debris-flow Hazards and*  
792 *Related Phenomena*. Berlin, Heidelberg: Springer Berlin Heidelberg, pp. 445–487. Available at:  
793 [https://link.springer.com/content/pdf/10.1007/3-540-27129-5\\_18.pdf](https://link.springer.com/content/pdf/10.1007/3-540-27129-5_18.pdf)  
794
- 795 Ivanov, P., Geological Institute, Bulgarian Academy of Sciences, Acad. Georgi Bonchev Str., Bl. 24, 1113  
796 Sofia, Bulgaria, Dobrev, N., Berov, B., Frantzova, A., Krastanov, M., Nankin, R., Geological Institute,  
797 Bulgarian Academy of Sciences, Acad. Georgi Bonchev Str., Bl. 24, 1113 Sofia, Bulgaria, & Geological  
798 Institute, Bulgarian Academy of Sciences, Acad. Georgi Bonchev Str., Bl. 24, 1113 Sofia, Bulgaria. (2022).  
799 Landslide risk for the territory of Bulgaria by administrative districts. *Geologica Balkanica*, 51(3), 21–28.  
800 <https://doi.org/10.52321/geolbalc.51.3.21>  
801
- 802 Iverson, R.M., Schilling, S.R, and Vallance, J.W., 1998, Objective delineation of areas at risk from inundation  
803 by lahars: *Geological Society of America Bulletin*, V 110, no.8, p. 972-984.
- 804 Jiang, W., Deng, Y., Tang, Z., Cao, R., Chen, Z. and Jia, K. 2016. Adaptive capacity of mountainous rural  
805 communities under restructuring to geological disasters: The case of Yunnan Province. *Journal of rural*  
806 *studies* 47, pp. 622–629. Available at: <http://dx.doi.org/10.1016/j.jrurstud.2016.05.002>.
- 807 Kean, J.W. et al. 2019. Inundation, flow dynamics, and damage in the 9 January 2018 Montecito debris-flow  
808 event, California, USA: Opportunities and challenges for post-wildfire risk assessment. *Geosphere* 15(4), pp.  
809 1140–1163. Available at: <http://dx.doi.org/10.1130/ges02048.1>.
- 810 Li, C., Wang, M. and Liu, K. 2018. A decadal evolution of landslides and debris flows after the Wenchuan  
811 earthquake. *Geomorphology (Amsterdam, Netherlands)* 323, pp. 1–12. Available at:  
812 <http://dx.doi.org/10.1016/j.geomorph.2018.09.010>.
- 813 Li, N., Tang, C., Zhang, X., Chang, M., Shu, Z. and Bu, X. 2021b. Characteristics of the disastrous debris flow  
814 of Chediguan gully in Yinxing town, Sichuan Province, on August 20, 2019. *Scientific reports* 11(1). Available  
815 at: <https://www.nature.com/articles/s41598-021-03125-x>
- 816 Li, Y. et al. 2024. Assessment of debris flow risk in Mentougou District, Beijing, based on runoff of potential  
817 debris flow. *Frontiers in earth science* 12. Available at: <http://dx.doi.org/10.3389/feart.2024.1426980>.
- 818 Liu, J., You, Y., Chen, X., Liu, J. and Chen, X. 2014. Characteristics and hazard prediction of large-scale  
819 debris flow of Xiaojia Gully in Yingxiu Town, Sichuan Province, China. *Engineering geology* 180, pp. 55–67.  
820 Available at: <https://www.sciencedirect.com/science/article/pii/S0013795214000702>
- 821 Liu, J., You, Y., Chen, X. and Chen, X. 2016. Mitigation planning based on the prediction of river blocking by  
822 a typical large-scale debris flow in the Wenchuan earthquake area. *Landslides* 13(5), pp. 1231–1242. Available  
823 at: <http://dx.doi.org/10.1007/s10346-015-0615-0>
- 824 Liu, J., Mason, P.J. and Bryant, E.C. 2018. Regional assessment of geohazard recovery eight years after the  
825 Mw7.9 Wenchuan earthquake: a remote-sensing investigation of the Beichuan region. *International journal of*  
826 *remote sensing* 39(6), pp. 1671–1695. Available at: <http://dx.doi.org/10.1080/01431161.2017.1410299>.
- 827 Luo, H.Y., Fan, R.L., Wang, H.J., and Zhang, L.M. 2020. Physics of building vulnerability to debris flows,  
828 floods, and earth flows. *Engineering geology* 271(105611), p. 105611. Available at:  
829 <https://www.sciencedirect.com/science/article/pii/S0013795219322227>.
- 830 Luo, H.Y., Zhang, L.M., Zhang, L.L., He, J., and Yin, K.S. 2023. Vulnerability of buildings to landslides: The  
831 state of the art and future needs. *Earth-science reviews* 238(104329), p. 104329. Available at:  
832 <https://www.sciencedirect.com/science/article/pii/S0012825223000181>.

833 Mattia Marconcini, Annekatriin Metz-Marconcini, Thomas Esch and Noel Gorelick. Understanding Current  
834 Trends in Global Urbanisation - The World Settlement Footprint Suite. *GI\_Forum* 2021, Issue 1, 33-38  
835 (2021) <https://austriaca.at/Oxc1aa5576%200x003c9b4c.pdf>

836 McGuire, L.A., Rengers, F.K., Kean, J.W. and Staley, D.M. 2017. Debris flow initiation by runoff in a recently  
837 burned basin: Is grain-by-grain sediment bulking or en masse failure to blame?: DEBRIS FLOW  
838 INITIATION. *Geophysical research letters* 44(14), pp. 7310–7319. Available at:  
839 <http://dx.doi.org/10.1002/2017gl074243>.

840 OpenStreetMap contributors. OpenStreetMap database [PostgreSQL via API]. OpenStreetMap Foundation:  
841 Cambridge, UK. 2024 [cited 20 Jul 2023]. © OpenStreetMap contributors. Available under the Open Database  
842 Licence from: [openstreetmap.org](https://www.openstreetmap.org). Data mining by Overpass turbo. Available at <https://www.openstreetmap.org>

843 Papathoma-Köhle, M., Kappes, M., Keiler, M. and Glade, T. 2011. Physical vulnerability assessment for alpine  
844 hazards: state of the art and future needs. *Natural hazards (Dordrecht, Netherlands)* 58(2), pp. 645–680.  
845 Available at: <http://dx.doi.org/10.1007/s11069-010-9632-4>.

846 Peng, M., Zhang, L.M., Chang, D.S. and Shi, Z.M. 2014. Engineering risk mitigation measures for the landslide  
847 dams induced by the 2008 Wenchuan earthquake. *Engineering geology* 180, pp. 68–84. Available at:  
848 <https://www.sciencedirect.com/science/article/pii/S0013795214000696>.  
849

850 Petley, D. 2023. *The 27 June 2023 landslide at Miansi, Sichuan Province, China*. Available at:  
851 <https://blogs.agu.org/landslideblog/2023/06/29/miansi-landslide-1/>  
852

853 Shen, P., Zhang, L. M., Chen, H. X., & Gao, L. (2017). Role of vegetation restoration in mitigating hillslope  
854 erosion and debris flows. *Engineering Geology*, 216, 122–133. <https://doi.org/10.1016/j.enggeo.2016.11.019>

855 Shu, B., Chen, Y., Amani-Beni, M. and Zhang, R. 2022. Spatial distribution and influencing factors of  
856 mountainous geological disasters in southwest China: A fine-scale multi-type assessment. *Frontiers in*  
857 *environmental science* 10. Available at: <http://dx.doi.org/10.3389/fenvs.2022.1049333>.

858 Tang, C., Rengers, N., van Asch, T.W.J., Yang, Y.H. and Wang, G.F. 2011. Triggering conditions and  
859 depositional characteristics of a disastrous debris flow event in Zhouqu city, Gansu Province, northwestern  
860 China. *Natural hazards and earth system sciences* 11(11), pp. 2903–2912. Available at:  
861 <https://nhess.copernicus.org/articles/11/2903/2011/nhess-11-2903-2011.pdf>.  
862

863 Tang, C., Van Westen, C.J., Tanyas, H. and Jetten, V.G. 2016. Analysing post-earthquake landslide activity  
864 using multi-temporal landslide inventories near the epicentral area of the 2008 Wenchuan earthquake. *Natural*  
865 *hazards and earth system sciences* 16(12), pp. 2641–2655. Available at: [http://dx.doi.org/10.5194/nhess-16-](http://dx.doi.org/10.5194/nhess-16-2641-2016)  
866 [2641-2016](http://dx.doi.org/10.5194/nhess-16-2641-2016).  
867

868 Tang, Y. et al. 2022. Assessing debris flow risk at a catchment scale for an economic decision based on the  
869 LiDAR DEM and numerical simulation. *Frontiers in earth science* 10. Available at:  
870 <http://dx.doi.org/10.3389/feart.2022.821735>  
871

872 Thouret, J.-C., Antoine, S., Magill, C. and Ollier, C. 2020. Lahars and debris flows: Characteristics and  
873 impacts. *Earth-science reviews* 201(103003), p. 103003. Available at:  
874 <http://dx.doi.org/10.1016/j.earscirev.2019.103003>.  
875

876 Wang, C., Li, S. and Esaki, T. 2008. GIS-based two-dimensional numerical simulation of rainfall-induced  
877 debris flow. Available at: <https://nhess.copernicus.org/articles/8/47/2008/nhess-8-47-2008.pdf>

878 Wei, L., Hu, K. and Liu, J. 2022. Automatic identification of buildings vulnerable to debris flows in Sichuan  
879 Province, China, by GIS analysis and Deep Encoding Network methods. *Journal of flood risk*  
880 *management* 15(4). Available at: <http://dx.doi.org/10.1111/jfr3.12830>

881 Wei, L., Hu, K., Liu, S., Ning, L., Zhang, X., Zhang, Q. and Rahim, M.A. 2024. The vulnerability of buildings  
882 to a large-scale debris flow and outburst flood hazard cascade that occurred on 30 August 2020 in Ganluo,

- 883 southwest China. *Natural hazards and earth system sciences* 24(11), pp. 4179–4197. Available at:  
884 <http://dx.doi.org/10.5194/nhess-24-4179-2024>.
- 885 Wei, L., Hu, K. and Liu, J. 2021 ‘Quantitative analysis of the debris flow societal risk to people inside buildings  
886 at different times: A case study of Luomo Village, Sichuan, Southwest China’, *Frontiers in Earth Science*, 8.  
887 doi:10.3389/feart.2020.627070.
- 888 Wei, L., Hu, K.-H. and Hu, X.-D. 2018. Rainfall occurrence and its relation to flood damage in China from  
889 2000 to 2015. *Journal of mountain science* 15(11), pp. 2492–2504. Available at:  
890 <http://dx.doi.org/10.1007/s11629-018-4931-4>
- 891 World Settlement Footprint Evolution data (1985-2015) ©DLR [cited Jul 2023]. 2019 All rights  
892 reserved. <https://geoservice.dlr.de/web/maps/eoc:wsfevolution>  
893
- 894 Wu, Y., Liu, X., Wang, J., Liu, L. and Shi, P. 2016. Landslide and debris flow disasters in China.  
895 In: *IHDP/Future Earth-Integrated Risk Governance Project Series*. Berlin, Heidelberg: Springer Berlin  
896 Heidelberg, pp. 73–101.  
897
- 898 Yan, Y., Ge, Y.G., Zhang, J.Q. and Zeng, C. 2014. Research on the debris flow hazards in Cutou Gully,  
899 Wenchuan County on July 10, 2013. *Journal of Catastrophology*, 29(3), pp.229-234.  
900
- 901 Yang, Y., Tang, C., Tang, C., Chen, M., Cai, Y., Bu, X. and Liu, C. 2023. Spatial and temporal evolution of  
902 long-term debris flow activity and the dynamic influence of condition factors in the Wenchuan earthquake-  
903 affected area, Sichuan, China. *Geomorphology (Amsterdam, Netherlands)* 435(108755), p. 108755. Available  
904 at: <http://dx.doi.org/10.1016/j.geomorph.2023.108755>.
- 905 Zeng, Q.L., Yue, Z.Q., Yang, Z.F. and Zhang, X.J. 2009. A case study of long-term field performance of  
906 check-dams in mitigation of soil erosion in Jiangjia stream, China. *Environmental geology* 58(4), pp. 897–911.  
907 Available at: <http://dx.doi.org/10.1007/s00254-008-1570-z>.
- 908 Zeng, C., Cui, P., Su, Z., Lei, Y. and Chen, R. 2015. Failure modes of reinforced concrete columns of buildings  
909 under debris flow impact. *Landslides* 12(3), pp. 561–571. Available at: <http://dx.doi.org/10.1007/s10346-014-0490-0>  
910
- 911 Zhang, S. 2014. Assessment of human risks posed by cascading landslides in the Wenchuan earthquake area.  
912 (Hong Kong): Hong Kong University of Science and Technology.
- 913 Zhang, Z. and Li, Y. 2020. Coupling coordination and spatiotemporal dynamic evolution between urbanization  
914 and geological hazards—A case study from China. *The Science of the total environment* 728(138825), p.  
915 138825. Available at: <http://dx.doi.org/10.1016/j.scitotenv.2020.138825>.
- 916 Zhu, Cheng, Bao, Chen, and Huang 2022. Shaking table tests on the seismic response of slopes to near-fault  
917 ground motion. *Geomechanics and engineering* 29(2), pp. 133–143. Available at:  
918 <http://dx.doi.org/10.12989/gae.2022.29.2.133>.
- 919 Zou, Q., Cui, P., He, J., Lei, Y. and Li, S. 2019. Regional risk assessment of debris flows in China—An HRU-  
920 based approach. *Geomorphology (Amsterdam, Netherlands)* 340, pp. 84–102. Available at:  
921 <https://www.sciencedirect.com/science/article/pii/S0169555X19301849>  
922  
923  
924  
925

## 926 **Statements & Declarations**

### 927 **Conflict of Interest**

928 The authors disclose no financial or non-financial interests of competing interest during the preparation of this  
929 manuscript.  
930  
931

932 **Author Contribution**

933 All authors contributed to the study conception and design. Material preparation, data collection and analysis were  
934 performed by Isabelle Utley, Tristram Hales and Ekbal Hussain. The first draft of the manuscript was written by  
935 Isabelle Utley and all authors commented on previous versions of the manuscript. All authors read and approved  
936 the final manuscript  
937